Proceedings of the Project Review, Geo-Mathematical Imaging Group (Purdue University, West Lafayette IN), Vol. 1 (2011) pp. 253-266.

THE EFFECT OF SATURATION ON SHEAR WAVE ANISOTROPY IN A TRANSVERSELY ISOTROPIC MEDIUM

WEIWEI LI*, CHRISTOPHER PETROVITCH†, AND LAURA J. PYRAK-NOLTE‡

Abstract. An experimental and theoretical study was performed to investigate the effect of saturation on compressional and shear wave anisotropy in a transversely isotropic medium. Experiments were performed on samples of Austin Chalk, a carbonate rock with fabric-controlled layering. Samples were saturated with either water or silicone oil. The theoretical approach was based on Backus Averaging for layered media and Gassmann's Equation for saturation. Modeling the sample as an effective medium captured most of the phenomenon observed in the experimental data such as a reduction in compressional wave velocity upon saturation and that the modulus measured by a shear wave propagated parallel to layers increased with increasing fluid viscosity. However, it was unable to predict the shear wave velocity for waves with a polarization perpendicular, Sv, to the layering. The Sv wave velocity indicated that the modulus associated with this shear-mode was weakened upon saturation.

1. Introduction. Carbonate rocks play a major economic role in the oil and gas industry. Over 50% of the world's oil reserves are contained in carbonate and the potential for additional gas reserve in these reservoirs is enormous. However, understanding and quantifying the physical properties and processes that occur in carbonate reservoirs is complicated because heterogeneity in physical properties occurs on all length scales in carbonate reservoirs, i.e., from the micro-scale to the reservoir scale. The complexity of structural and textural composition of the rock arises from depositional processes, post-depositional diagenetic processes and bio-geo-chemical interactions (i.e., dissolution and replacement by newly formed phases). The major constituents in the rock (e.g., fossils, ooides, etc) and the packing and cementation of these constituents result in heterogeneity in physical properties at multiple scales.

In this paper, we investigate the effect of fabric-controlled layering in a carbonate rock on seismic anisotropy and if the measured anisotropy is affected by fluid saturation.

2. Theory.

2.1. Thomsen's Parameter. The simplest anisotropic model with broad geophysical applicability is known as transverse isotropy (TI) or hexagonal symmetry. This model has been used to model shear wave anisotropy caused by layering [1] as well as by a set of parallel fractures [2]. Transverse isotropy for a layered rock means that the rock is isotropic within any plane normal to the axis of layering, i.e. the axis of rotation symmetry [3]. Planes parallel to the axis of rotation exhibit shear wave anisotropy for shear waves polarized perpendicular and parallel to the layers. For a transversely isotropic system, the elastic stiffness tensor has five independent constants:

$$\begin{pmatrix} c_{11} & c_{12} & c_{13} & 0 & 0 & 0 \\ c_{12} & c_{11} & c_{13} & 0 & 0 & 0 \\ c_{13} & c_{13} & c_{33} & 0 & 0 & 0 \\ 0 & 0 & 0 & c_{44} & 0 & 0 \\ 0 & 0 & 0 & 0 & c_{44} & 0 \\ 0 & 0 & 0 & 0 & 0 & c_{66} \end{pmatrix} \tag{2.1}$$

$$c_{66} = \frac{1}{2}(c_{11} - c_{12})$$

*Department of Physics, Purdue University, West Lafayette, Indiana, USA
†Department of Physics, Purdue University, West Lafayette, Indiana, USA
‡Department of Physics, Purdue University, West Lafayette, Indiana, USA, and Department of Earth and Atmospheric Physics, Purdue University, West Lafayette, Indiana, USA and School of Civil Engineering, Purdue University, West Lafayette, Indiana, USA

In a transversely isotropic medium, there are three modes of propagation: quasi-longitudinal, quasi-shear and pure shear. The velocities of the three modes are given as:

$$
\begin{aligned}
V_{qP}(\theta) &= \sqrt{\frac{c_{11}\sin^2(\theta) + c_{33}\cos^2(\theta) + c_{44} + \sqrt{M(\theta)}}{2\rho}} \\
V_{qSV}(\theta) &= \sqrt{\frac{c_{11}\sin^2(\theta) + c_{33}\cos^2(\theta) + c_{44} - \sqrt{M(\theta)}}{2\rho}} \\
V_{SH}(\theta) &= \sqrt{\frac{c_{66}\sin^2(\theta) + c_{44}\cos^2(\theta)}{\rho}} \\
M(\theta) &= \left[(c_{11} - c_{44})\sin^2(\theta) - (c_{33} - c_{44})\cos^2(\theta)\right]^2 + (c_{13} + c_{44})^2 \sin^2(2\theta)
\end{aligned}
\tag{2.2}
$$

where θ is the angle between the wave vector and the axis of symmetry. And the five components of the stiffness tensor can be obtained from five velocity measurement: $V_{qP}(0°), V_{qP}(90°), V_{qP}(45°)$, $V_{SH}(90°)$ and $V_{SH}(0°) = V_{qSV}(90°)$.

Thomsen [4] noted that most rocks encountered in reservoirs exhibited weak anisotropy and introduced the following parameters to describe weak anisotropy:

$$
\begin{aligned}
\varepsilon &= \frac{c_{11} - c_{33}}{2c_{33}} \\
\delta &= \frac{(c_{13} + c_{44})^2 - (c_{33} - c_{44})^2}{2c_{33}(c_{33} - c_{44})} \\
\gamma &= \frac{c_{66} - c_{44}}{2c_{44}}
\end{aligned}
\tag{2.3}
$$

The constant ε describes the fractional difference between the P-wave velocities in the vertical and horizontal directions, i.e. propagation directions perpendicular and parallel to the layering, respectively. The constant γ describes the fractional difference between the SH-wave (pure shear wave) velocities between vertical and horizontal directions, which is equivalent to the difference between the vertical and horizontal polarizations of the horizontally propagating S-waves (i.e., propagating direction parallel to the layers). One interpretation of the constant δ is that it represents the difference between the P-wave and Sv-wave anisotropies [5].

2.2. Backus Averaging. One approach for determining the effective elastic constants for a thinly layered medium is the method of Backus [6]. The medium can be composed of either isotropic or anisotropic layers. In the long-wavelength limit, a transversely isotropic rock composed of layers can be represented by an anisotropic effective medium defined by an effective stiffness as follows:

$$
\begin{pmatrix}
A & B & F & & & \\
B & A & F & & & \\
F & F & C & & & \\
 & & & D & & \\
 & & & & D & \\
 & & & & & M
\end{pmatrix}
\tag{2.4}
$$

where

$$
\begin{aligned}
M &= \frac{1}{2}(A - B) \\
A &= \left\langle a - f^2 c^{-1} \right\rangle + \left\langle c^{-1} \right\rangle^{-1} \left\langle f c^{-1} \right\rangle^2 \\
B &= \left\langle b - f^2 c^{-1} \right\rangle + \left\langle c^{-1} \right\rangle^{-1} \left\langle f c^{-1} \right\rangle^2
\end{aligned}
\tag{2.5}
$$

$$C = \left\langle c^{-1} \right\rangle^{-1}$$
$$F = \left\langle c^{-1} \right\rangle^{-1} \left\langle f c^{-1} \right\rangle$$
$$D = \left\langle d^{-1} \right\rangle^{-1}$$
$$M = \langle m \rangle$$

a, b, c, d and f are five independent elastic constants of layer components and brackets $\langle \cdot \rangle$ indicate the average of the enclosed properties weighted by their volumetric proportions.

If the individual layers are isotropic, the number of independent constants needed to describe each individual layer is reduced to 2 and these constants can be calculated in terms of the P and S wave velocities and densities:

$$a = c = \lambda + 2\mu = \rho V_P^2 \tag{2.6}$$
$$d = m = \mu = \rho V_S^2$$
$$b = f = \lambda = \rho \left(V_P^2 - V_S^2 \right)$$

2.3. Gassmann's Relation. Gassmann's fluid substitution relation is commonly applied to predict the bulk modulus for the saturated rock with different fluids:

$$\frac{K_{sat}}{K_0 - K_{sat}} = \frac{K_{dry}}{K_0 - K_{dry}} + \frac{K_{fl}}{\phi \left(K_0 - K_{fl} \right)} \tag{2.7}$$
$$\mu_{sat} = \mu_{dry}$$

Gassmann's equation estimates the saturated bulk modulus (K_{sat}) through the bulk modulus of the forming minerals (K_0), the bulk modulus of the frame or dry rock (K_{dry}), the bulk modulus of the fluid (K_{fl}) and the rock porosity (ϕ) [7].

3. Experiment Procedure. Two different experimental approaches were used to examine the anisotropy of a layered carbonate rock and the effect of fluid substitution on the observed anisotropy. These approaches are described below along with a description of the samples.

3.1. Layer Resulted Anisotropy Measurement. Laboratory measurements were performed on samples of Austin Chalk Cordova Cream obtained from Texas Quarries, Inc. Diagenetic and chemical processes resulted in the formation of fine bedding that results in a weakly directed fabric. Two Austin Chalk samples, AC11 and AC12, were quasi-cylindrical in shape with a diameter of 4 inches. Around the circumference of the sample, 32 flats were machined along the length of the sample (Figure 1). The centers of the flats were approximately 11 degrees apart. The locations of the planes were chosen such that the top and bottom flats were perpendicular to the layering in the samples. All the sides were labeled from side 1 to side 32. Green dots on each side marked the position of ultrasonic transducers.

Contact piezoelectric transducers were used to send and receive compressional and shear waves through the sample. The transducers had a central frequency of 1 MHz. The shear wave measurements were made for both polarizations, parallel to the flat and perpendicular to the long axis of the flat. The transducers were measured in pairs, i.e. a source and receiver were diametrically opposed during data acquisition. This procedure was used for all 32 flats.

3.2. Fluid Substitution Measurement. Prisms (50 mm by 50 mm by 100 mm) and small cubic samples (with each edge $\sim$ 50 mm) were used in these experiment sets (Figure 2 (a) and (b)). Dimensions of samples and saturation method used are listed in appendix table. Some samples coated with marine epoxy were imbibed with fluid at constant infusing rate 1ml/hr and the others were vacuum saturated.

Figure 2(c) shows a sketch of experiment setup for the fluid substitution experiments. In Figure 2(c), the orange dashed lines represent the orientation of the layers (all of the layers are not shown). All samples were labeled and oriented during the experiments such that sides with the same labels

(a) Top view of AC12 showing the fine layering in the sample.

(b) Side view of AC12 showing machined flats.

FIG. 1. *Photographs of Austin Chalk.*

have the same layer orientation. The grey circles represent the positions of transducers. The red arrows represent two independent polarizations of shear wave that were measured. Compressional and shear waves were propagated from side C to side A, side D to side B, and side E to side F.

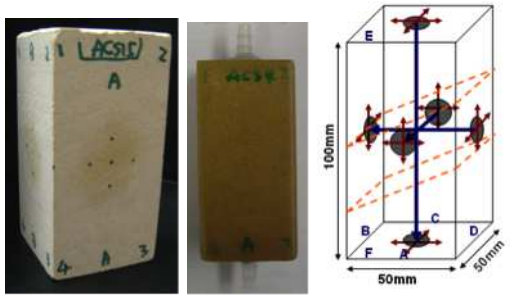

FIG. 2. *(a) and (b) Digital images of prismatic samples ACS15 and ACS4 coated with marine epoxy, (c) A sketch of the experimental set-up for the fluid substitution experiments.*

4. Model. A two-layer components model was developed to study the layer-induced transverse isotropy by applying Backus Averaging and Gassmann's Equation. The parameters used in this study are listed in Table 4.1. The values in Table 4.1 are based on our laboratory measurements [8]. For a given porosity of each layer, the corresponding density of each layer was calculated base on the following equation:

$$\rho_i = \rho_o(1-\phi_i) + \rho_{fl}\phi_i \tag{4.1}$$

where is the density of calcite, is the density of pore fluid and is the porosity of the layer. The assumed properties of calcite are listed in Table 4.2.

	Volume Proportion	Porosity	P Velocity (m/s)	S Velocity (m/s)
Layer 1	50%	25%	3000	1800
Layer 2	50%	20%	4200	2650

TABLE 4.1
Layer Parameters used in the model

Calcite density	Calcite Bulk Modulus	Water density	Water Bulk Modulus
2710 (kg/m3)	76.8 GPa	1000 (kg/m3)	2.15 GPa

TABLE 4.2
Layer Parameters used in the model [9]

5. Results and discussion.

5.1. Layer Resulted Anisotropy Results. Thomsen parameters were calculated for samples AC11 and AC12 and are listed in Table 5.1. All of the parameters are less than 1 and indicate the rock has weak anisotropy. The anisotropy of AC11 is slightly less than that of AC12. AC11 may be less anisotropic because it had more uniform layering than sample AC12. From Figure 1, the layers in AC12 are not parallel. The layer spacing is smaller on one side of the sample compared to the other side. From Berryman [10] and Helbig [11], if anisotropy is caused by fine layering of isotropic materials, then strictly $\delta < \varepsilon$ (isotropic layers). Thus it could be claimed that Austin Chalk displayed weak anisotropy based on the Thomsen parameters. However, the anisotropy of AC12 is not purely transversely isotropic.

	AC11 Dry	AC11 wet	AC12 dry	AC12 wet	Model dry	Model wet
ε	0.0626	0.0558	0.1313	0.1099	0.0698	0.0440
δ	-0.0809	-0.0572	0.1572	0.1386	-0.0149	-0.0295
γ	0.0227	0.0287	0.0861	0.0906	0.0931	0.0931

TABLE 5.1
Thomsen Parameters for AC11, AC12 and the Model

When comparing the results from the model to those from AC11, it was found that there exist both similarities and differences. Both the model and data exhibited a decrease in ε after saturation with water. However, the model and AC11 showed different trends with saturations for the δ and γ parameters. The δ parameter for AC11 increased while model yielded a decrease in δ with saturation. For γ, the AC11 value increased with saturation while γ of the model remained unchanged.

P wave anisotropy is described by ε and is defined as the difference between P velocities propagation perpendicular and parallel to layer plane. Upon fluid saturation, the amount of P wave anisotropy decreased. Though a long wavelength approximation was used, this observed change in ε would yield reflection coefficients that would indicate that the P wave impedance contrast was altered by water saturation, i.e. the P wave anisotropy decreased.

γ is the difference between S_H velocities propagated perpendicular and parallel to the layer planes, and thus describes S_H wave anisotropy. The model predicts no change in γ with saturation, however AC11 yielded an increase in γ. From the fluid substitution experiment sets, the behavior of the γ parameter varied, i.e. sometimes it decreased, remain unchanged or increased. A detailed discussion of this is in the next section.

Velocity surfaces for the P- and S-waves were reconstructed according to the calculated Thomsen Parameters of AC11 (Figure 3). The reconstructed velocity surfaces from the model matches the P and S_H experimental result quite well, but does not match measured S_V velocity surface. The calculated experimental δ does not capture the behavior of AC11. But both model and experiment value of δ are negative in sign.

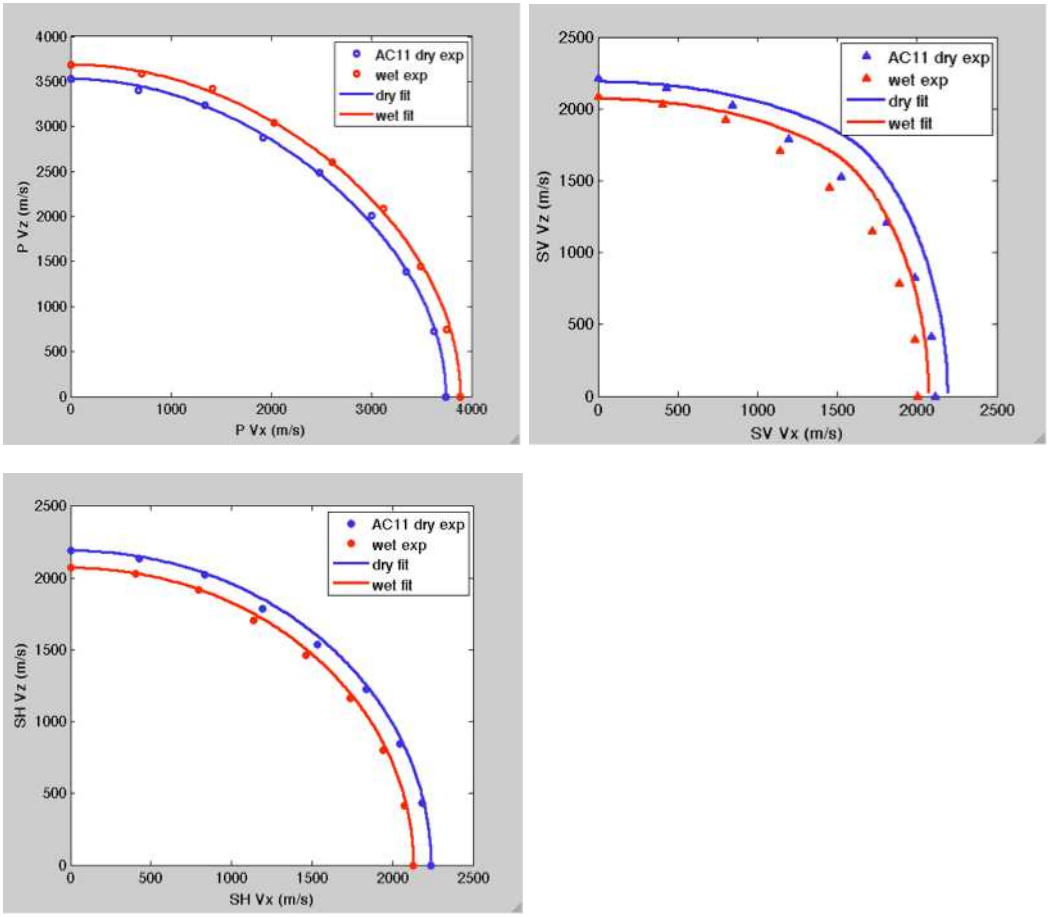

FIG. 3. *Velocity surfaces for dry and wet P-, S_V- and S_H- waves.*

Effect of saturation on seismic velocity as a function of incident angle is shown in Figure 4. Symbols and solid lines represent the experimental data and model results, respectively. From the model, The P-wave velocity increased and the S-wave velocities decreased upon saturation.

The experimental results show a similar trend. The P-wave velocity increased the most for near vertical incidence and reaches a minimum when P-wave was propagated parallel to layering. The S_V–wave velocity decreased upon saturation with the minimum value occurring at an incident angle of ~ 50. Sv velocities from AC11 decreased the most for propagation directions that were parallel or perpendicular to the layering. The model shows that saturation results in a decrease in S_H wave velocity but the decrease is the same for all angles of incident. The measured ratio of dry and wet S_H wave velocities varied around the model value.

Based on the comparison to the model, if only the P- and S_H wave data were used, the Austin Chalk samples could be treated as a transversely isotropic medium. For example, water saturation reduced the P wave anisotropy, and the changes in the P- and S- wave velocities upon saturation showed similar trends as a function of incident angle dependence as the theoretical prediction. However, the S_V-wave behavior deviated from the theoretical predictions based on transverse isotropy. One hypothesis for these deviations for the S_V-wave is that an effective medium model is not applicable at the experimental wavelengths for these Austin Chalk samples. The S_V-wave has the slowest velocity and the shortest wavelength relative to the P-wave and S_H-wave. The wavelength of the S_V-wave at 1 MHz is on the order of 2 mm, i.e. approaching the assumed thickness of the layers 1 – 1.5 mm. Another possible is scattering caused by heterogeneity within the sample. Li

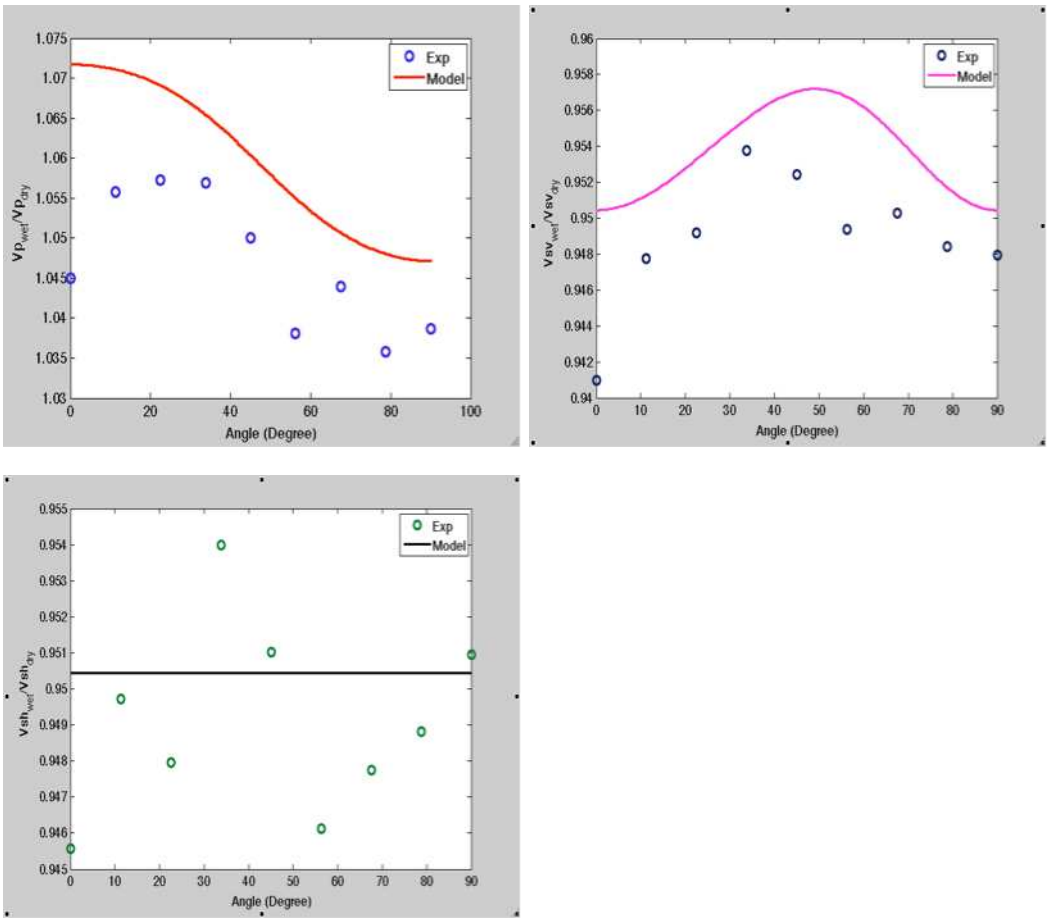

FIG. 4. *Ratio of dry and wet P-, S_V- and S_H- velocity as a function of incident angle*

et al. [8] showed from X-ray tomographic scans that the layers in Austin Chalk varied in density with the density varying along the layers. For Sv-wave propagation, the sample may be more complicated than a simple transversely isotropic model.

5.2. Fluid Substitution Results. As mentioned in the experimental sections, shear waves were propagated through the prismatic and cubic samples in three orthogonal directions for compressional waves and for both polarizations of shear waves. Table 5.2 lists the sample name, dimensions of the sample and the method used to saturate the sample. From the measurements from side C to side A, we determined that the two independent polarizations of shear waves did not align with the layering in the sample but were aligned were parallel to top and bottom surfaces for 0 degrees and for 90 degrees were aligned parallel to side surfaces. The transversely isotropic symmetric plane did not match the layer plane but is tilted roughly 15 degrees from the normal to the layers. The symmetry axis is perpendicular to side E and side F, not perpendicular to layer plane. Therefore, the layering structure partially contributes to sample's anisotropy but other factors possibly during diagenesis, or other physical processes have lead to an orientation of the rock constituents (pellets, fossils, etc.) may also contribute the sample's anisotropy.

Shear-wave velocities, corresponding shear modulus and calculated gamma parameters upon water and silicone oil saturation are shown in Figure 5 and Figure 6, respectively. In these Figures, the horizontal axis lists the sample name. Note that the last two letters in the sample name indicate the propagation direction of this S-wave (see Figure 2(c)). Samples ACS8, NTA, ACS5

	C to A (mm)	D to B (mm)	Saturation Method
ACS8	50	47	Imbibed
NTA2	51.2	49	Vacuum
ACS14	48.9	49.5	Vacuum
ACS5	51	50	Imbibed
ACS6	46	48	Imbibed
ACS15	49.59	49.30	Vacuum
ACS16	50.09	48.84	Vacuum

TABLE 5.2
Samples Dimensions and Saturation Method

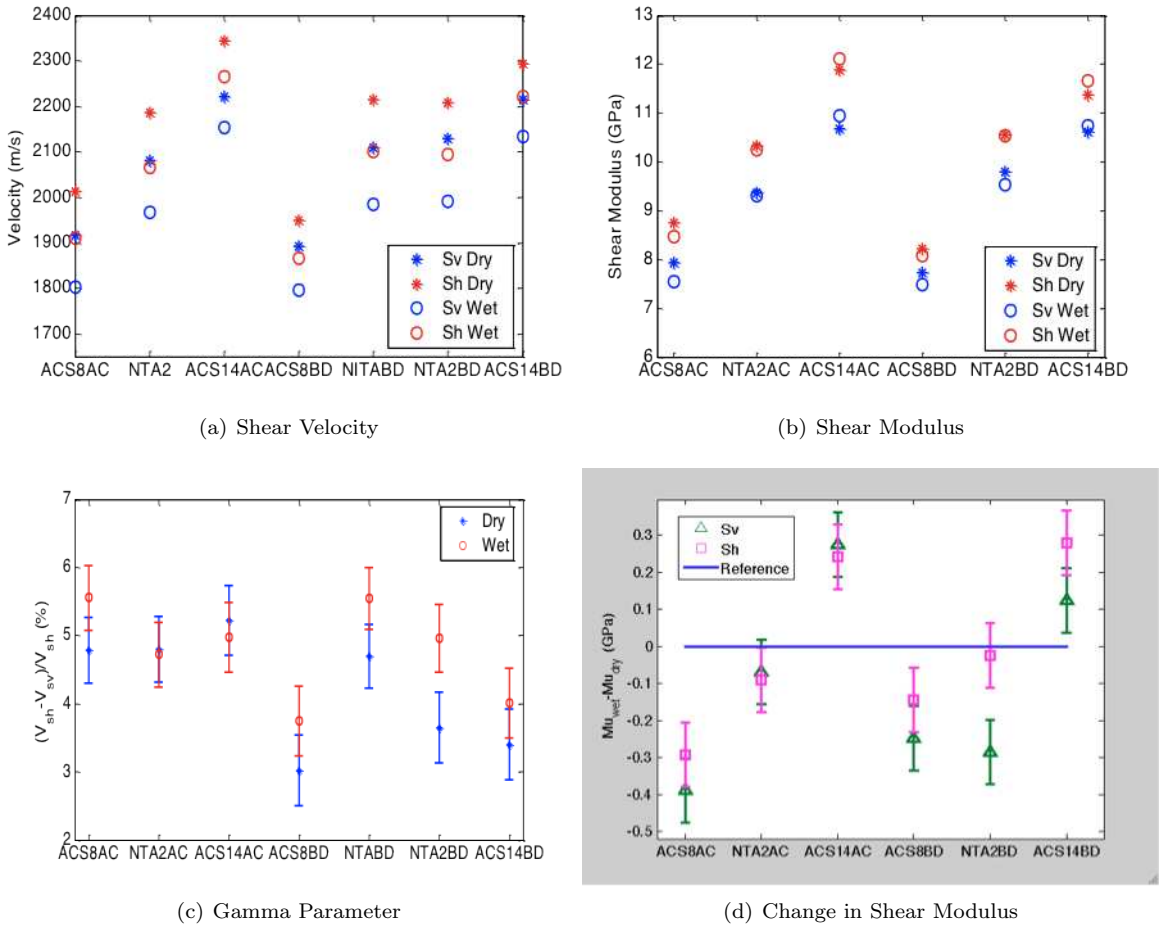

(a) Shear Velocity

(b) Shear Modulus

(c) Gamma Parameter

(d) Change in Shear Modulus

FIG. 5. *Shear velocities, modulus and gamma parameter upon water saturation.*

and ACS6 were saturated using an imbibition method. Samples NTA2, ACS14, ACS15 and ACS16 were vacuum saturated.

From the experimental data, it could be concluded that three factors affect the shear modulus and S_H wave anisotropy: the saturation method, wave propagation direction relative to the layers (C to A or D to B) and the saturating fluid. From Figure 2(c), the propagation direction from C to A was parallel to layering while the propagation direction from D to B was across the layering with incident angle around 70 degrees.

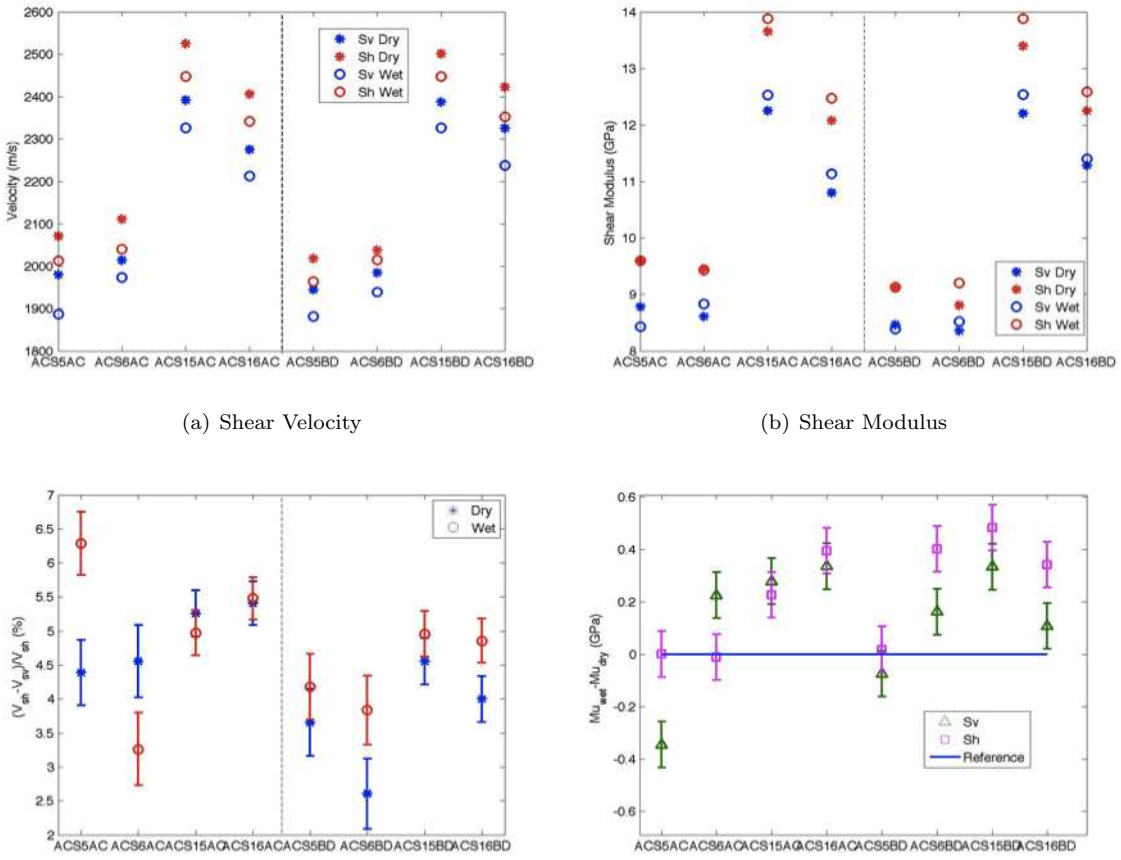

(a) Shear Velocity

(b) Shear Modulus

(c) Gamma Parameter

(d) Change in Shear Modulus

FIG. 6. *Shear velocities, modulus and gamma parameter upon silicone oil saturation.*

First, we examine the results for shear waves propagated through side C to side A. Gamma parameter exhibits a larger difference between the dry and saturated case when the samples were imbibed compared to those that were vacuum saturated samples. This indicates that imbibition method did not result in a uniformly saturated sample. Although the infusion rate was 1ml/hr, air could still be trapped during fluid invasion cause scattering of seismic waves. Vacuum saturation provided a more uniform saturation of the connected pore spaces.

The velocity of S_H wave in a transversely isotropic medium depends on c_{44} and c_{66} from Equation (2.2). In the layer-induced transversely isotropic case, we have:

$$c_{44} = \left\langle \frac{1}{\mu} \right\rangle^{-1} \tag{5.1}$$
$$c_{66} = \langle \mu \rangle$$

It is obvious that c_{44} and c_{66} only depend on the shear modulus μ of each layer. Gassmann's equation states that $\mu_{sat} = \mu_{dry}$ with fluid substitution and thus the shear modulus of a transversely isotropic medium will change upon saturation, i.e. c_{44} and c_{66} remain constant. The Thomsen parameter γ also only depends on c_{44} and c_{66} (Equation 2.3) and also leads the conclusion that S_H wave anisotropy remain unchanged upon saturation.

Gassmann's equation is applicable at low frequency. In the ultrasonic frequency range (1MHz),

there isn't enough time for the pore pressure to equilibrate and thus Gassmann's equation will underpredict the elastic modulus. From the experimental data, water-saturated samples exhibited a decrease in shear modulus, while silicone oil-saturated samples showed an increased in shear modulus (for data from propagation direction C to A in the fully saturated case).

Possible mechanisms that can cause weakening or strengthening of carbonate are: (1) opening or close of low aspect ratio of pore and cracks; (2) viscous-coupling between the fluid and the rock and (3) dissolution of carbonates minerals. In our experiment, no confining pressure is applied to the sample and mechanisms (1) cannot be the reason for shear modulus deviation. Comparing the shear modulus of the samples saturated with water and silicone oil, an obvious increase in shear modulus was observed in the samples saturated with silicone oil. This could be caused by the so called 'Low-Flow Mechanism' or 'Squirt-flow Mechanism' [12,13]. Such mechanism tends to happen when a rock is saturated with a high viscosity fluid. This explains why Austin chalk saturated with silicone oil exhibited shear stiffening effect. The viscosity of the silicon oil was 5 times that of water. Dissolution of minerals is another plausible explanation for the decrease in shear modulus upon water saturation. The distilled water used for saturation process had a PH value of around 4 and therefore displays a weak acidity. Thus there is a possibility that calcite mineral dissolved during saturation. The dissolution would cause chemical weakening and a reduction in shear modulus.

We also examined the effect of angle of incidence on the interpreting the effect of fluid substitution for a layered sample. We observed that there exists incident angle dependence in the change in S_V and S_H shear modulus no matter what type of fluid was used for saturation. Only considering samples fully saturated (vacuum saturated), the change in the S_V modulus and the change in the S_H modulus were similar when shear waves were propagated from side C to side A parallel to layers (Figure 5(d) NTA2AC, ACS14AC; Figure 6(d) ACS15AC, ACS16AC). However, the difference between the S_V modulus and the S_H modulus increased when shear waves were propagated from side D to side B with an incident angle around 70 degree (Figure 5(d) NTA2BD, ACS14BD; Figure 6(d) ACS15BD, ACS16BD). If the S_H modulus decreased, then the S_V modulus decreased more (NTA2BD). If the S_H modulus increased, then the S_V modulus showed less of an increase (ACS14BD, ACS15BD, ACS16BD). This means that no change in the γ parameter was observed for waves propagated from side C to side A, and an increase in the γ parameter occurred for waves propagated from side D to side B.

The effect of saturation on the shear modulus and the γ parameter as a function of incident angle from the model are shown in Figure 7. Please pay attention to this γ parameter. When the propagation direction is not parallel to layer plane, γ is calculated from the following equation:

$$\gamma = \frac{\nu_{SH}(\theta) - \nu_{SV}(\theta)}{\nu_{SH}(\theta)} \tag{5.2}$$

Equation (5.2) does not describe the SH wave anisotropy. The γ parameter in Equation (5.2) describes the normalized velocity difference between S_H and S_V wave. We still call it γ for convenience. From the model, the S_V modulus never decreases and S_H modulus is constant (Figure 7a). γ is zero at normal incidence and reaches a maximum at 90 degree incidence for S_V. No matter what the incident angle is, the γ parameters of the wet case cannot be larger than γ parameters of the dry case (Figure 7b).

However, the data from the experiments do not exactly confirm these predictions. First, let's focus on the shear wave propagating parallel to layering structure (model: 90 degree incidence; experiment: side C to side A). The theoretical model predicts that (for an angle of incidence of 90 degrees) after saturation both S_H and S_V moduli remain unchanged as well as the γ parameter (Figure 7 a & b). From the experiments, we observed that both S_H and S_V modulus changed (decreased or increased) upon saturation (see Figure 5d samples NTA2AC and ACS14AC; Figure 6d samples ACS15AC and ACS16AC), but the γ parameter remained the same (see Figure 5c NTA2AC and ACS14AC; Figure 6c ACS15AC and ACS16AC). The reason that the γ parameter did not change upon saturation of the samples is that the S_H and S_V modulus changed almost the same amount upon silicone oil or water saturation in the experiments. From equation (2.2), it is

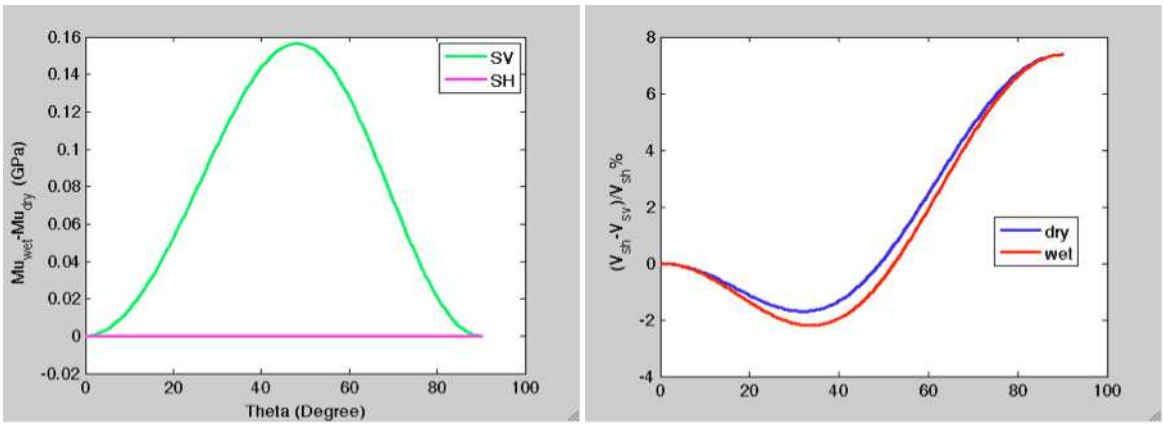

(a) Change in Shear Modulus (b) Equation (5.2) Gamma Parameter

FIG. 7. *Change of shear modulus and gamma parameter upon saturation, as a function of incident angle.*

clear that at 90 degrees incidence, S_H and S_V waves are purely shear mode and only depend on c_{66} and c_{44}, separately. It is predicted that $c_{66}$and c_{44} should remain unchanged upon saturation. Possible reasons for this deviation from the shear modulus predicted by the theory were discussed in section earlier in this section. Now, given the fact that deviation exists, this comparable change of S_H and S_V modulus in experiments indicates that change of elastic constant c_{66} and c_{44} of Austin Chalk are similar upon saturation.

Next, let's focus on the shear wave propagating across layering (model: 70 degree incidence; experiment: side D to side B). The theoretical model predicts that after saturation the S_H modulus should not change while the S_V modulus should increase (Figure 7a). The unchanged S_H modulus and increased S_V modulus results in a decrease in the γ parameter (Figure 7b). This was not observed in the experimental data. In the experiments, when the S_H modulus decreased, the S_V modulus decreased more (Figure 5d NTA2BD). When the S_H modulus increased, the S_V modulus showed less of an increase (Figure 5d ACS14BD and Figure 6d ACS15BD and ACS16BD). This resulted an increase in the γ parameter in experiments, rather than the decrease predicted by the model (Figure 5c NTA2BD and ACS14BD; Figure 6c ACS15BD andACS16BD). From equation (2.2), it is clear that at 70 degree incidence, the S_H wave is still a purely shear mode and depends on both c_{66} and c_{44} but the S_V wave is not. The S_V wave contains other elastic constants of the stiffness tensor c_{11}, c_{13}, c_{33} in addition to c_{44}. From the theoretical predication, the combined effect of c_{11}, c_{13}, c_{33} should increase S_V modulus with another prediction that c_{44}remain the same upon saturation. The observed less change of S_V modulus than change of S_H modulus in experiments indicates that the combined effect of c_{11}, c_{13}, c_{33} did not change the same relative amount at that experienced by c_{44} and c_{66}.

6. Conclusion. According to the experiment data and the model, the Thomsen parameters for Austin Chalk are less than 1 indicating that this type of carbonate rock is weakly anisotropic. Using the Backus Averaging method, we were able to reconstruct the seismic velocity surfaces from the experimental data. The reconstructed P-wave and S_H wave velocity surfaces fit the measured results quite well. However, the reconstructed S_V wave velocity surface did not match the measured data. The wavelength of the S_V-wave is roughly 2 mm, which is close to the thickness of the layers in the sample. This suggest that sample can be treated as an effective medium for predicting the P- and S_H-wave velocities but not for S_V-waves for these Austin Chalk samples.

For P-wave and S_H wave, Austin Chalk can be described as a transversely isotropic medium generally. Using Backus averaging and Gassmann's equations, a theoretical model was able to predict the general trend of velocity behavior upon saturation. Both the experimental and the

model results showed that fluid saturation causes a decrease in P wave anisotropy.

From our study of the effect of saturation, as a function of angle incidence, on P-, S_H – and S_V – wave velocities, we observed that the general trends predicted by the theory but the sample response was more complicated, i.e., the data did not vary smoothly as a function of angle of incidence. The deviation as a function of angle incidence suggest that the wavelength to layer thickness ratio is such that long wavelength approximation cannot be used or treated as an effective medium.

In the fluid substitution experiments, behavior of the S_H modulus upon saturation was observed to deviate from the behavior predicted from Gassmann's equations. A high viscosity fluid resulted in stiffening of rock frame and an increase in shear modulus, while water produced softening of the rock frame, possibly caused by mineral dissolution or grain contact weakening. At 70 degrees incidence angle, the difference between the change in the S_V modulus and the S_H modulus increased while the theory predicted a decrease. This contradiction arises because elastic moduli other than shear moduli (c_{11}, c_{13}, c_{33}) play a role in S_V modulus while only shear moduli play a role in S_H modulus (c_{44} and c_{66}). The combined effect of c_{11}, c_{13}, c_{33} did not change the relative amount with regards to the amount changed of c_{44} and c_{66}.

While Backus Averaging and Gassmann's Prediction can capture the basic features of the Austin Chalk with weak transverse isotropy, it cannot capture alterations caused by geochemical interactions or heterogeneous structure (i.e. gain alignment, non-uniform layers and scattering among layers) that approaches the wavelength of the signal. However, this may not be possible on the laboratory scale or the field scale. On the reservoir scale, carbonate reservoirs exhibit heterogeneity but may not exhibit any known anisotropic model because of interlaced as well as discontinuous rock units with various orientations caused by the depositional environmental and diagenetic processes. Thus, it is important to develop numerical models that can cross-scales of structural complexity.

7. Acknowledgements. The authors wish to acknowledge support of this work by the Geosciences Research Program, Office of Basic Energy Sciences US Department of Energy (DE-FG02-09ER16022), by Exxon Mobil Upstream Research Company and the Geo-Mathematical Imaging Group at Purdue University

References.

1. Crampin, S. A. 1977. A review of the effects of anisotropic layering on the propagation of seismic waves. *Geophys. J. R. Astr. Soc.* 49, 9-27.
2. Pyrak-Nolte, L.J., L.R. Myer, and N.G.W. Cook. 1990. Anisotropy in seismic velocities and amplitudes from multiple parallel fractures. *Journal of Geophysical Research-Solid Earth and Planets* **95**(B7) p. 11345-11358.
3. Jaeger, J.C., Cook, N.G.W. and R. W. Zimmerman. 2007. *Fundamentals of Rock Mechanics.* Fourth Edition. Blackwell Publishing. Oxford, U.K. p142-143.
4. Thomsen, L. 1986. Weak elastic anisotropy. *Geophysics* 51, 1954–1966. Hazzard, J.F., R.P. Young, and S.C. Maxwell. 2000. Micromechanical modeling of cracking and failure in brittle rocks. *J. Geophys. Res.* 105: 16,683–16,697.
5. Banik, N. C. 1987. An effective anisotropy parameter in transversely isotropic media. *Geophysics.* 52, 1654-1664.
6. Backus, G.E. 1962. Long-wave elastic anisotropy produced by horizontal layering. *Journal of Geophysical Research* 67: 4427-4440.
7. Gassmann, F. 1951, Uber die elastizität poröser medien: Vierteljahrsschrift der Naturforschenden Gesellschaft in Zürich, 96, 23.
8. Li, W. Petrovitch, C. and L. J. Pyrak-Nolte. 2009. The effect of fabric-controlled layering on compressional and shear wave propagation in carbonate rock. *International Journal of the Japanese Commmittee for Rock Mechanics.* 4(2) Nov 2009, pp79-85.
9. Mavko, G. T. Mukerji and J. Dvorkin. 1998. *The Rock Physics Handbook.* Cambrige.
10. Berryman, J. G. 1979. Long-wave elastic anisotropy in transversely isotropic media. *Geophysics* 65 (5): 1627-1629.

11. Helbig, K. 1979. Discussion on " The reflection, refraction and diffraction of waves in media with elliptical velocity dependence" by F. K. Levitt. *Geophysics* 44: 987-990.
12. Akbar N. Dvorkin J. and Nur A. 1993. Relating P-wave attenuation to permeability. *Geophysics* 58: 20-29.
13. Mavko G. and Nur A. 1979. Wave attenuation in partially saturated rocks. *Geophysics* 44: 161-178.